

Observation of magnetic structural universality using transverse NMR relaxation

Alexander Ruh,^{1,2} Philipp Emerich,¹ Harald Scherer,³ Dmitry S. Novikov,⁴ and Valerij G. Kiselev^{1,*}

¹*Medical Physics, Department of Radiology, Medical Center - University of Freiburg,
Faculty of Medicine, University of Freiburg, Freiburg, Germany*

²*Department of Radiology, Feinberg School of Medicine, Northwestern University, Chicago, IL, USA*

³*Institute of Inorganic and Analytical Chemistry, University of Freiburg, Freiburg, Germany*

⁴*Bernard and Irene Schwartz Center for Biomedical Imaging, Department of Radiology,
New York University School of Medicine, New York, NY, USA*

(Dated: August 18, 2021)

Transverse NMR relaxation from spins diffusing through a random magnetic medium is sensitive to its structure on a mesoscopic scale. In particular, this results in the time-dependent relaxation rate. We show analytically and numerically that this rate approaches the long-time limit in a power-law fashion, with the exponent reflecting the disorder class of mesoscopic magnetic structure. The spectral line shape acquires a corresponding non-analytic power law singularity at zero frequency. We experimentally detect a change in the dynamical exponent as a result of the transition into a maximally random jammed state characterized by hyperuniform correlations.

Transverse NMR or EPR relaxation is sensitive to the spectral density of the fluctuating environment.¹⁻⁴ Such environment can emerge when the spins travel across magnetically disordered media, such as semiconductors,^{5,6} porous rocks,^{7,8} and biological tissues.⁹⁻¹⁴ While the magnetic structure remains static, the stochastic motion of spins enables sampling its spatial fluctuations, resulting in a non-Lorentzian spectral line-shape and a time-dependent relaxation rate.¹⁵⁻²¹

Here we show that this rate approaches the long-time limit in a power-law fashion, and relate its dynamical exponent to the structural exponent²² characterizing long-range spatial correlations of magnetic structure. In particular, we experimentally observe a change in the dynamical exponent as a result of the transition into a maximally random jammed state²³ characterized by hyperuniform correlations.^{24,25} Our results reflect the hierarchical nature of structural complexity contributing to a macroscopic NMR signal: its functional form is defined by the structural universality class, whereas microscopic parameters affect the nonuniversal coefficients. The relation between relaxational dynamics and magnetic structure opens the way for noninvasive characterization of porous media, complex materials and biological tissues.

The transverse NMR relaxation signal is given by the average of the precession phase factor $s(t) = \langle e^{-i\varphi(t)} \rangle$, $\varphi = \int_0^t \Omega(\tau) d\tau$, where $\Omega(\tau)$ is the fluctuating Larmor frequency offset experienced by nuclear spins. This averaging for times $t \gg t_c$ exceeding the correlation time t_c of $\Omega(t)$ falls into the realm of the central limit theorem:^{2,5} the signal is asymptotically determined by its second-order cumulant $\ln s(t) \approx -\langle \varphi^2 \rangle / 2 \sim -\langle \varphi_1^2 \rangle \cdot (t/t_c)$, where $\langle \varphi_1^2 \rangle$ is the phase variance on a single correlated “step”, and these variances add up on the path split into a large number $\sim t/t_c$ of uncorrelated steps. For a weak dephasing, the resulting relaxation rate $R_2 \sim \langle \varphi_1^2 \rangle / t_c \sim \langle \Omega^2 \rangle t_c$ is the essence of the motional-narrowing picture of Anderson and Weiss,² which applies to the dipole-dipole interaction between the excited spins on a molecular scale. Such monoexponential molecular relaxation emerges from the enormous separation of scales between the correlation time $t_c \sim 1 - 10$ ps of molecular motion and the typical NMR measurement time scale $t \sim 1 - 100$ ms.

In this work, we consider the loss of Larmor precession coherence in media with a static magnetic structure on a much larger, *mesoscopic* scale⁹⁻¹¹ relevant for NMR experiments in porous rocks^{7,8} and in biological tissues.¹²⁻²¹ Here, the individual precession phases $\varphi(t) = \int_0^t \Omega(\mathbf{r}_\tau) d\tau$ decohere due to the path-dependent Larmor frequency offset $\Omega(\mathbf{r}_\tau)$ on their Brownian trajectories \mathbf{r}_τ induced by heterogeneous medium’s magnetic susceptibility. The macroscopic $t \rightarrow \infty$ rate $R_2^\infty \sim \langle \Omega^2(\mathbf{r}) \rangle t_c$ decreases for a faster diffusion constant D , as the time $t_c \sim l_c^2/D$ to travel across the disorder correlation length l_c shortens, exemplifying the diffusion narrowing.^{14,16,17,26} Importantly, the typical mesoscopic correlation times t_c can be of the order of the NMR measurement time scale, which makes it possible to explore the *transient* signal evolution $s(t)$ before the long-time monoexponential limit is reached, via studying the corresponding time-dependent relaxation rate $R_2(t) = -d \ln s(t)/dt$.

The mesoscopic contribution to the transverse relaxation, in principle, depends on myriads of parameters characterizing the spatial organization of susceptibility-induced $\Omega(\mathbf{r})$. It is generally non-universal, and sensitive to the shape of magnetic inclusions (e.g. cells).^{18,27} Our main result is the *universal* feature of the mesoscopic relaxation which manifests itself in the power-law tail in the approach of $R_2(t)$ to R_2^∞ ,

$$\frac{dR_2}{dt} \sim t^{-\nu} \quad \text{for } t \gg t_c \quad (1)$$

such that $R_2^\infty - R_2(t) \sim t^{-\nu+1}$ for $\nu > 1$, and $R_2(t) \sim \ln t$ for $\nu = 1$; an upper temporal limit on this behavior is discussed below. We relate the dynamical relaxation exponent

$$\nu = \frac{p+d}{2} \quad (2)$$

to the large-scale statistics of the structural organization: The relevant signature of the d -dimensional medium, represented by magnetic susceptibility $\chi(\mathbf{r})$ varying on the mesoscopic scale, is embodied by the (magnetic) structural exponent p , which we define via the $k \rightarrow 0$ scaling of the power spectrum

$$\Gamma_2^X(k) = \int d^d \mathbf{r} e^{-i\mathbf{k}\mathbf{r}} \langle \chi(\mathbf{r}_0 + \mathbf{r}) \chi(\mathbf{r}_0) \rangle_{\mathbf{r}_0} \sim k^p, \quad k \rightarrow 0. \quad (3)$$

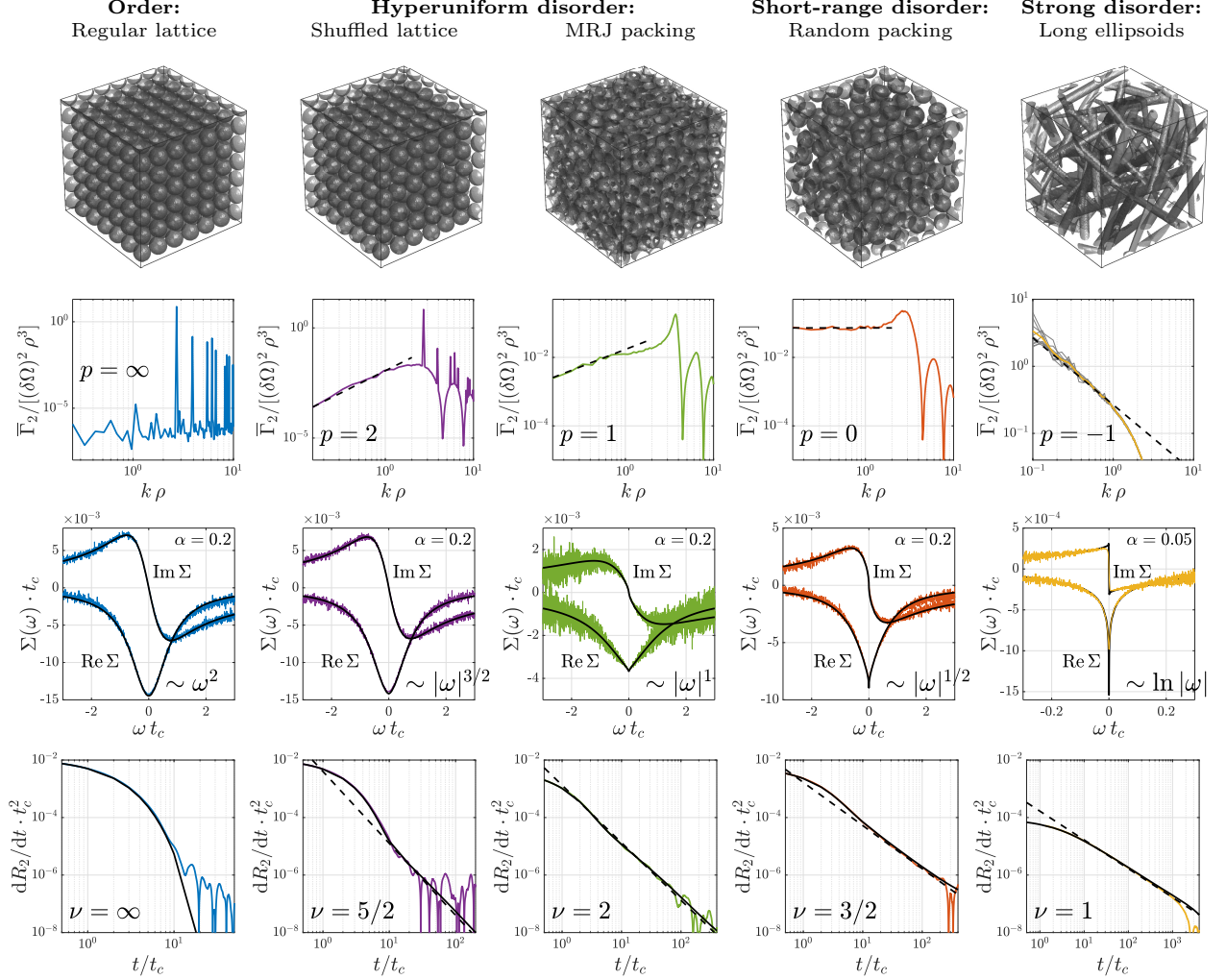


FIG. 1. **Illustration of the universality relations (1) – (3) for the disorder classes in $d = 3$ dimensions.** Columns show the results for five fully permeable synthetic media with qualitatively distinct structural fluctuations (see Methods). First row shows a quarter of the Monte Carlo simulation box in each dimension; second row shows the angular-averaged power spectra $\bar{\Gamma}_2(k)$, Eq. (4); third and fourth rows show the self-energy part $\Sigma(\omega)$ (see text) and $dR_2(t)/dt$, numerically obtained from the simulations. The packing of long ellipsoids has large fluctuations at small k . This is a finite-size effect that is alleviated by the ensemble averaging (thicker yellow line) over 10 disorder realizations (thin gray lines). $\Sigma(\omega)$ and $dR_2(t)/dt$ obtained from MC simulations (colors) are compared with the leading-order calculation (black lines) by integrating the numerically found power spectra according to Eqs. (9) and (10), respectively, while neglecting R_2^∞ on the right-hand side. For $dR_2(t)/dt$ (fourth row) this agrees well with the asymptotic limit (1) with the exponent (2) (dashed lines). Parameters ρ , $\delta\Omega$, α , and t_c are defined in Methods.

The exponent p takes a few discrete values,²² characterizing distinct universality classes of structural disorder.

The key relation (2) is illustrated in Fig. 1 for five statistically isotropic disorder classes in $d = 3$ dimensions using Monte Carlo (MC) simulations, where we identify the exponent p in the angular-averaged power spectra

$$\bar{\Gamma}_2(k) = \frac{\langle \Omega_{-\mathbf{k}} \Omega_{\mathbf{k}} \rangle_{\hat{\mathbf{k}}}}{V} = c_d (4\pi\gamma B_0)^2 \cdot \Gamma_2^\chi(k) \sim k^p \quad (4)$$

of the susceptibility-induced Larmor frequency offset^{18,28} $\Omega_{\mathbf{k}} = 4\pi\gamma B_0 \chi_{\mathbf{k}} Y_{\hat{\mathbf{k}}}$ (Fig. 2), where $Y_{\hat{\mathbf{k}}} = 1/3 - k_z^2/k^2$ is the elementary dipole field, γB_0 is the average Larmor frequency, and V is the sample volume. The scaling of the power spectra

of the structure and of the induced frequency with $k = |\mathbf{k}|$ is similar²¹ due to the $Y(\mathbf{r}) \sim 1/r^d$ dependence of the dipole field, with $c_3 = \langle |Y_{\hat{\mathbf{k}}}|^2 \rangle_{\hat{\mathbf{k}}} = 4/45$, meaning that the transverse relaxation effectively samples the structure of the medium (i.e. $\chi(\mathbf{r})$) *directly*, even though it senses the induced $\Omega(\mathbf{r})$.

The universality (2) in the diffusion-narrowing regime can be used as a probe of the global structural organization of magnetically heterogeneous media, and for the mesoscopic model selection. In Fig. 1, four kinds of identical sphere arrangements, and one with randomly placed long (prolate) ellipsoids, represent five distinct universality classes. In particular: *Order*, represented by a cubic lattice of spheres, shows no long-range fluctuations and $\bar{\Gamma}_2(k) \equiv 0$ for small k , which

can be associated with an exponent $p = \infty$, yielding an exponentially fast decay of dR_2/dt (faster than any inverse power law). For *hyperuniform disorder*,²⁴ $p > 0$, these fluctuations are not completely absent but are suppressed. Examples are a *shuffled lattice*,²⁹ where the lattice objects are randomly displaced from their original positions, showing a quadratic behavior $\overline{\Gamma}_2|_{k \rightarrow 0} \sim k^2$, with $p = 2$ yielding $\nu = 5/2$; and a *maximally random jammed (MRJ) packing*,²³ where $\overline{\Gamma}_2|_{k \rightarrow 0} \sim k$, with a nontrivial exponent²⁵ $p = 1$, which manifests itself in $dR_2/dt \sim 1/t^2$. *Short-range disorder* (the most widespread disorder class, characterized by a finite correlation length, e.g. as in the Poissonian objects' placement) is represented here by the random packing of non-overlapping spheres. Its power spectrum is characterized by a finite plateau at small k , $\overline{\Gamma}_2(k)|_{k \rightarrow 0} = \text{const}$, such that $p = 0$ and $\nu = d/2$. Finally, *strong disorder* is characterized by the diverging structural fluctuations resulting in the exponent $p < 0$. An example are randomly placed "rods", such as vessels or capillaries in the brain (here represented by highly prolate ellipsoids whose long axis exceeds the range of diffusion lengths), yielding $\overline{\Gamma}_2|_{k \rightarrow 0} \sim k^{-1}$, $p = -1$, such that $\nu = 1$ and the relaxation rate $R_2(t) \sim \ln t$ diverges.

In what follows, we will provide a qualitative coarse-graining argument for the universal relation (2), Fig. 2, followed by the self-consistent approximation (10) for the signal, Fig. 3, and then demonstrate experimentally how the change of the disorder universality class due to the jamming transition, $p = 0 \rightarrow p = 1$, can be detected via the dynamics (1) of the measured bulk transverse relaxation, Fig. 4.

An intuition behind the relation of dR_2/dt to the spatial fluctuations stems from realizing that the time t defines the diffusion length scale $L(t) = \sqrt{2dDt}$, which acts as a coarse-graining window for the Larmor frequency, $\Omega(\mathbf{r}) \rightarrow \Omega_t(\mathbf{r})$, effectively "seen" by the spins, Fig. 2. If we were to begin the evolution of magnetization at such t foregoing shorter times, then the coarse-grained $\Omega_t(\mathbf{r})$ would have the effective correlation length $L(t) > l_c$, and the variance $\langle \Omega_t^2(\mathbf{r}) \rangle \sim \langle \Omega^2(\mathbf{r}) \rangle [l_c/L(t)]^d$ decreasing as $t^{-d/2}$ for the short-range disorder due to Poissonian statistics. We now apply the conventional diffusion-narrowing argument $dR_2/dt_c \sim \langle \Omega^2 \rangle$ to our effective $\Omega_t(\mathbf{r})$, by identifying $t_c \rightarrow t$ and $\langle \Omega^2 \rangle \rightarrow \langle \Omega_t^2 \rangle$:

$$\frac{dR_2(t)}{dt} \approx \langle \Omega_t^2(\mathbf{r}) \rangle \sim t^{-\nu}, \quad (5)$$

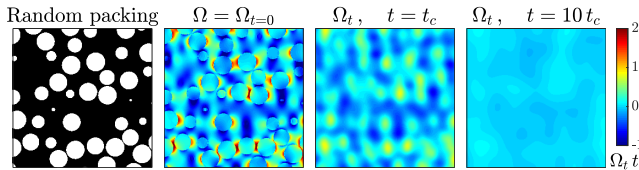


FIG. 2. **Larmor frequency offset and its coarse-graining by diffusion.** A section through the 3d random sphere packing from the fourth column in Fig. 1: The Larmor frequency $\Omega(\mathbf{r}) \equiv \Omega_{t=0}(\mathbf{r})$ induced by the distinct magnetic susceptibility assigned to the spheres, and the coarse-grained $\Omega_t(\mathbf{r})$ for $t = t_c$ and $10t_c$. The coarse-graining occurs via the local averaging of the frequency over the length $L(t) \sim \sqrt{Dt}$.

with $\nu = d/2$ for the Poissonian case of $p = 0$.

One can view Eq. (5) as a real-space renormalization group equation on the effective macroscopic parameter R_2 over the increasing diffusion length scale $L(t)$. We immediately see that the rate $R_2(t)$ *always increases* with t , as each length scale contributes a strictly positive frequency variance to the relaxation; however, its growth slows down due to the self-averaging, as the instantaneous distribution $\Omega_t(\mathbf{r})$ becomes narrower with t , Fig. 2. Moreover, the self-averaging will be faster when the fluctuations $\langle \Omega_t^2(\mathbf{r}) \rangle$ decrease faster than the inverse "diffusion volume" $L^{-d}(t)$ (which happens for hyperuniform media,²⁴ $p > 0$), and slower for strong disorder with diverging fluctuations, $p < 0$, in agreement with Fig. 1.

This "RG flow" must eventually stop for $t > t_*$ such that $t_*R_2(t_*) \sim 1$, when $R_2(t)$ becomes so large that the mesoscopic signal is suppressed exponentially before spins can sample fluctuations of $\Omega(\mathbf{r})$ at the scales exceeding $L(t_*)$. After $t > t_*$, the power law (1) gets cut-off, Fig. 3, and by then the mesoscopic signal $s(t) \ll 1$. Hence, the scaling (1) is detectable for $t_c \ll t \lesssim t_*$, provided that the relaxation is sufficiently weak, i.e. $R_2(t_c)t_c \ll 1$, which is equivalent to a small "single-step" phase variance $\langle \varphi_1^2 \rangle \sim \langle \Omega^2(\mathbf{r}) \rangle t_c^2 \ll 1$.

The above intuition is supported by finding the disorder-averaged Green's function $G_{t,\mathbf{r}-\mathbf{r}_0} = \langle \mathcal{G}_{t,\mathbf{r},\mathbf{r}_0} \rangle$ of the mesoscopic Bloch-Torrey equation for the transverse nuclear magnetization^{14,21,30}

$$[\partial_t - \partial_{\mathbf{r}} D(\mathbf{r}) \partial_{\mathbf{r}} + i\Omega(\mathbf{r})] \mathcal{G}_{t,\mathbf{r},\mathbf{r}_0} = \delta(t) \delta(\mathbf{r} - \mathbf{r}_0), \quad (6)$$

where $D(\mathbf{r})$ is the local diffusion coefficient. The mesoscopic contribution $s(t)$ to the NMR signal is helpful to think of in terms of "spin packets", the groups of spins emanating from the same point \mathbf{r}_0 . The magnetization of a spin packet is $\int d\mathbf{r} \mathcal{G}_{t,\mathbf{r},\mathbf{r}_0}$; the \mathbf{r}_0 - and t -dependence of this quantity embodies the coarse-graining discussed above. Acquisition from a macroscopic sample entails ensemble-averaging of the spin packet magnetization, $s(t) = \frac{1}{V} \int d\mathbf{r} d\mathbf{r}_0 \mathcal{G}_{t,\mathbf{r},\mathbf{r}_0} \equiv \int d\mathbf{r} G_{t,\mathbf{r}}$. In other words, the signal $s(t) \equiv G_{t,\mathbf{q}}|_{\mathbf{q}=0}$ is the Fourier transform of $G_{t,\mathbf{q}}$ for the wavenumber $\mathbf{q} = 0$. Here and in what follows, we factor out the molecular relaxation; the experimentally observable signal $S(t) = e^{-R_2^{\text{mol}} t} s(t)$.

We represent the disorder-averaged propagator of Eq. (6)

$$G_{\omega,\mathbf{q}} = \frac{1}{-i\omega + D_{\infty} q^2 - \Sigma_{\omega,\mathbf{q}}} \quad (7)$$

in terms of the self-energy part^{21,31} $\Sigma_{\omega,\mathbf{q}}$ that collects all one-particle irreducible Feynman diagrams accounting for $\Omega(\mathbf{r})$ and the deviation $D(\mathbf{r}) - D_{\infty}$ from the macroscopic diffusion constant D_{∞} . The expansion of $\Sigma_{\omega,\mathbf{q}}$ in the powers of \mathbf{q} reflects the measurable mesoscopic effects in the bulk relaxation²¹ (due to even-order correlators $\langle \Omega(\mathbf{r}_1)\Omega(\mathbf{r}_2)\dots \rangle$), frequency shift (similar correlators of odd orders), diffusion³¹ (due to $\langle D(\mathbf{r}_1)D(\mathbf{r}_2)\dots \rangle$), and apparent diffusion³² (due to the cross-terms $\langle \Omega(\mathbf{r}_1)D(\mathbf{r}_2)\dots \rangle$). In particular, the mesoscopic spectral lineshape $s(\omega) = [-i\omega - \Sigma(\omega)]^{-1}$, where $\Sigma(\omega) \equiv \Sigma_{\omega,\mathbf{q}}|_{\mathbf{q}=0}$.

We consider the self-energy part in the self-consistent Born approximation,²¹ equivalent to summing up the "rainbow" di-

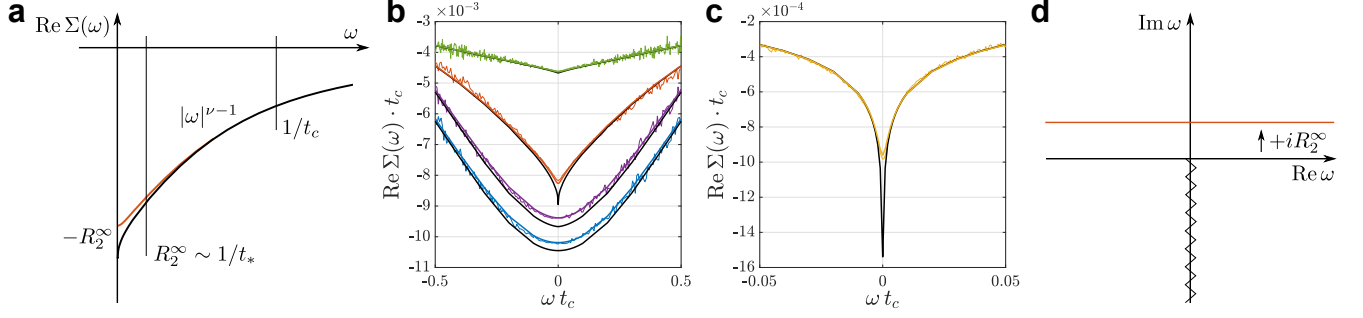


FIG. 3. **Self-consistent regularization of the $\omega \rightarrow 0$ behavior.** Panel (a) shows a schematic of $\Sigma(\omega)$ for small ω . Panels (b,c) show the zoomed low-frequency range from Fig. 1 using the same colors (lines vertically shifted for the readability). The thick noiseless colored curves depict the self-consistent correction, Eq. (9), to the leading-order calculation (black lines), resulting in a perfect agreement with simulations. Panel (d) depicts the sampling of $\Sigma(\omega)$ off the singularity at $\omega = 0$ due to the self-regularization for long times that results in a finite R_2^∞ .

agrams for $\Sigma_{\omega, \mathbf{q}}$:

$$\Sigma_{\omega, \mathbf{q}} \approx - \int \frac{d^d \mathbf{k}}{(2\pi)^d} \frac{\Gamma_2(\mathbf{k})}{-i\omega + D_\infty(\mathbf{q} + \mathbf{k})^2 - \Sigma_{\omega, \mathbf{q} + \mathbf{k}}}, \quad (8)$$

where the frequency power spectrum, Eq. (4), is taken before the angular averaging. The lowest-order approximation to Eq. (8) corresponds to neglecting $\Sigma_{\omega, \mathbf{q} + \mathbf{k}}$ on the right-hand side, thereby giving the conventional second-order perturbation theory in $\Omega(\mathbf{r})$,^{16–21} which is asymptotically exact in the diffusion narrowing limit. In this limit, the time domain quantity $\Sigma(t) = -dR_2(t)/dt$.

The next iteration, in the $\omega \rightarrow 0$ limit, is to set $\Sigma_{\omega, \mathbf{q} + \mathbf{k}} \rightarrow \Sigma(0) \approx -R_2^\infty$, the terminal relaxation rate, such that

$$\Sigma(\omega) \approx - \int \frac{d^d \mathbf{k}}{(2\pi)^d} \frac{\bar{\Gamma}_2(k)}{-i\omega + D_\infty k^2 + R_2^\infty}, \quad (9)$$

equivalent to the temporal scaling

$$\frac{d}{dt} R_2(t) \approx -\Sigma(t) \approx \int \frac{d^d k}{(2\pi)^d} \bar{\Gamma}_2(k) e^{-D_\infty k^2 t - R_2^\infty t}, \quad (10)$$

where the coarse-grained variance $\langle \Omega_t^2(\mathbf{r}) \rangle$ is just the Larmor frequency correlation function “filtered” by the diffusion propagator $e^{-D_\infty k^2 t}$, cf. Eq. (5). Hence, Fig. 2 has been obtained using the identification $\Omega_t(\mathbf{k}) = \Omega(\mathbf{k}) e^{-D_\infty k^2 t/2}$, which represents Gaussian smoothing over the diffusion length $L(t)$. Using the low- k scaling (4), we obtain Eqs. (1) and (2) for $t_c \ll t \lesssim t_*$. The result of leading-order numerical integration (according to Eq. (10) with R_2^∞ neglected) agrees well with MC simulations in Fig. 1 and with asymptotic scaling (1) for all considered disorder classes. The exponent $\nu = 1$ for long ellipsoids is equivalent to $\ln s(t) \sim -t \ln t$ for blood vessels.¹⁶ For $p = 0$, the scaling $dR_2/dt \sim t^{-3/2}$ agrees with the asymptotic behavior for the model medium of Jensen and Chandra¹⁷ and for diluted impermeable spheres analyzed by Sukstanskii and Yablonskiy.²⁰

Equivalently, for the leading-order self-energy part, cf. Eq. (9), we obtain for positive non-integer ν

$$\Sigma(\omega) - \Sigma(0) \sim - \frac{(-i\omega)^{\nu-1}}{\sin \pi \nu}, \quad (11)$$

where $-i = e^{-i\pi/2}$. For positive integer ν , $\Sigma(\omega) - \Sigma(0) \sim (i\omega)^{\nu-1} \ln(-i\omega)$ with account for the regularizing contribution of the region $k \gtrsim k_c$. This gives the specific pattern for $\omega \rightarrow 0$ shown in the third row in Fig. 1. These singularities compete with the regular contribution of the domain with finite k in the integral of Eq. (9) that gives $\text{Re } \Sigma(\omega) \sim \omega^2$ and $\text{Im } \Sigma(\omega) \sim \omega$. These terms define the form of $\Sigma(\omega)$ near $\omega = 0$ for the regular lattice and dominate $\text{Im } \Sigma(\omega)$ for the shuffled lattice ($\nu = 5/2$), Fig. 1.

Figure 1 demonstrates a good agreement between the numerically obtained leading-order singularities and MC simulations. A close look at very small frequencies, $\omega t_* \lesssim 1$ (Fig. 3), reveals a lack of accuracy, which is completely cured by the self-consistent Born approximation, Eq. (9). According to this equation, the regularization can be viewed as sampling of the leading-order $\Sigma(\omega)$ along the line $\text{Im } \omega = R_2^\infty$, missing the singularity at $\omega = 0$ in the complex plane of ω by the small value R_2^∞ (Fig. 3d). If $\Sigma(\omega)$ is measured without correcting for the molecular relaxation, this shift increases by the

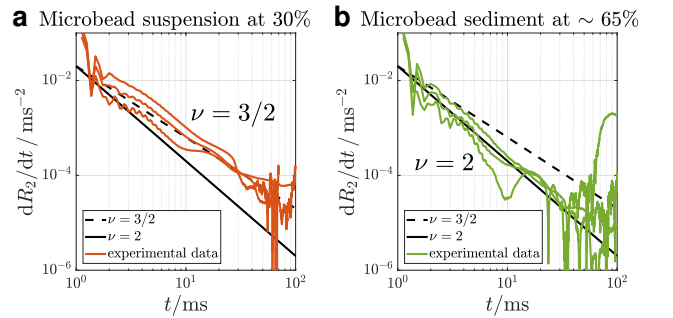


FIG. 4. **Experimental observation of transition into the MRJ state.** The dynamical exponent (2) changes from $\nu = 3/2$ to $\nu = 2$ in aqueous suspension of polystyrene microbeads, according to the change of the disorder universality class between the dilute suspension with short-range disorder, $p = 0$ (panel a), and an MRJ sediment with the predicted exponent²⁵ $p = 1$ (panel b). Shown are representative data sets for water doped with paramagnetic agent ($\text{HoCl}_3 \cdot 6\text{H}_2\text{O}$) with concentrations 1.5, 2.0 and 2.5 mmol/L to create a magnetic susceptibility contrast with the microbeads (see Methods for experimental details).

substitution $R_2^\infty \rightarrow R_2^{\text{mol}} + R_2^\infty$.

The present discussion shows that the universality, our main result expressed by Eqs. (1) and (2), is mapped onto the behavior of the structural power spectrum for small k , which is independent of individual properties of the magnetized objects. This is illustrated in supplementary Fig. S1 that shows results of MC simulations for the same media as in Fig. 1, but with the magnetized objects made *impermeable* for diffusing spins.

As an application of the developed formalism, in Fig. 4 we experimentally demonstrate the change of the disorder universality class $p = 0 \rightarrow 1$ after reaching the maximally random jammed state for mono-dispersed spheres, where the nontrivial exponent $p = 1$ was predicted numerically.²⁵ NMR relaxation in two microbead packings (suspension and densely-packed sediment) exhibit distinct exponents for the time derivative of the relaxation rate, which makes it possible to distinguish the two packings using a *macroscopic* NMR

measurement in contrast to the microscopic character of up-to-date observations.^{33–35} This remarkable sensitivity of the macroscopic measurement to the nontrivial mesoscopic structure is enabled by the time-dependent coarse-graining window, Fig. 2, that effectively samples the mesoscopic medium’s power spectrum (3).

To conclude, we have shown analytically and numerically, that the mesoscopic component of the transverse relaxation rate displays a universal scaling behavior that is sensitive to the statistics of large-scale organization of tissue magnetic susceptibility. This allowed us to provide the first macroscopic experimental observation of the MRJ transition in spherical microbead packings using NMR relaxation. Our results provide a framework for noninvasive investigation of the structure of complex materials and in biomedical magnetic resonance imaging, where both native and added susceptibility contrast is ubiquitous.

* valerij.kiselev@uniklinik-freiburg.de

- ¹ N. Bloembergen, E. M. Purcell, and R. V. Pound, “Relaxation Effects in Nuclear Magnetic Resonance Absorption,” *Phys Rev* **73**, 679–712 (1948).
- ² P. W. Anderson and P. R. Weiss, “Exchange Narrowing in Paramagnetic Resonance,” *Rev Mod Phys* **25**, 269–276 (1953).
- ³ A. V. Khaetskii, D. Loss, and L. Glazman, “Electron Spin Decoherence in Quantum Dots due to Interaction with Nuclei,” *Phys Rev Lett* **88**, 186802 (2002).
- ⁴ G. S. Uhrig, “Keeping a Quantum Bit Alive by Optimized π -Pulse Sequences,” *Phys Rev Lett* **98**, 100504 (2007).
- ⁵ M. I. D’yakonov and V. I. Perel’, “Spin orientation of electrons associated with the interband absorption of light in semiconductors,” *Sov Phys JETP* **33**, 1053–1059 (1971).
- ⁶ G. Salis, Y. Kato, K. Ensslin, D. C. Driscoll, A. C. Gossard, and D. D. Awschalom, “Electrical control of spin coherence in semiconductor nanostructures,” *Nature* **414**, 619–622 (2001).
- ⁷ M. D. Hürlimann, “Effective Gradients in Porous Media Due to Susceptibility Differences,” *J Magn Reson* **131**, 232–240 (1998).
- ⁸ Y.-Q. Song, S. Ryu, and P. N. Sen, “Determining multiple length scales in rocks,” *Nature* **406**, 178–181 (2000).
- ⁹ J. A. Glasel and K. H. Lee, “On the Interpretation of Water Nuclear Magnetic Resonance Relaxation Times in Heterogeneous Systems,” *J Am Chem Soc* **96**, 970–978 (1974).
- ¹⁰ K. R. Thulborn, J. C. Waterton, P. M. Matthews, and G. K. Radda, “Oxygenation dependence of the transverse relaxation time of water protons in whole blood at high field,” *Biochim Biophys Acta* **714**, 265–270 (1982).
- ¹¹ P. Gillis and S. H. Koenig, “Transverse Relaxation of Solvent Protons Induced by Magnetized Spheres: Application to Ferritin, Erythrocytes, and Magnetite,” *Magn Reson Med* **5**, 323–345 (1987).
- ¹² R. M. Weisskoff, C. S. Zuo, J. L. Boxerman, and B. R. Rosen, “Microscopic Susceptibility Variation and Transverse Relaxation: Theory and Experiment,” *Magn Reson Med* **31**, 601–610 (1994).
- ¹³ H. C. Davis, P. Ramesh, A. Bhatnagar, A. Lee-Gosselin, J. F. Barry, D. R. Glenn, R. L. Walsworth, and M. G. Shapiro, “Mapping the microscale origins of magnetic resonance image contrast with subcellular diamond magnetometry,” *Nat Commun* **9**, 131 (2018).
- ¹⁴ V. G. Kiselev and D. S. Novikov, “Transverse NMR relaxation in biological tissues,” *NeuroImage* (2018), 10.1016/j.neuroimage.2018.06.002.
- ¹⁵ D. A. Yablonskiy and E. M. Haacke, “Theory of NMR Signal Behavior in Magnetically Inhomogeneous Tissues: The Static Dephasing Regime,” *Magn Reson Med* **32**, 749–763 (1994).
- ¹⁶ V. G. Kiselev and S. Posse, “Analytical Theory of Susceptibility Induced NMR Signal Dephasing in a Cerebrovascular Network,” *Phys Rev Lett* **81**, 5696–5699 (1998).
- ¹⁷ J. H. Jensen and R. Chandra, “NMR Relaxation in Tissues With Weak Magnetic Inhomogeneities,” *Magn Reson Med* **44**, 144–156 (2000).
- ¹⁸ V. G. Kiselev and D. S. Novikov, “Transverse NMR Relaxation as a Probe of Mesoscopic Structure,” *Phys Rev Lett* **89**, 278101 (2002).
- ¹⁹ A. L. Sukstanskii and D. A. Yablonskiy, “Gaussian approximation in the theory of MR signal formation in the presence of structure-specific magnetic field inhomogeneities,” *J Magn Reson* **163**, 236–247 (2003).
- ²⁰ A. L. Sukstanskii and D. A. Yablonskiy, “Gaussian approximation in the theory of MR signal formation in the presence of structure-specific magnetic field inhomogeneities. Effects of impermeable susceptibility inclusions,” *J Magn Reson* **167**, 56–67 (2004).
- ²¹ D. S. Novikov and V. G. Kiselev, “Transverse NMR relaxation in magnetically heterogeneous media,” *J Magn Reson* **195**, 33–39 (2008).
- ²² D. S. Novikov, J. H. Jensen, J. A. Helpert, and E. Fieremans, “Revealing mesoscopic structural universality with diffusion,” *Proc Natl Acad Sci USA* **111**, 5088–5093 (2014).
- ²³ S. Torquato, T. M. Truskett, and P. G. Debenedetti, “Is Random Close Packing of Spheres Well Defined?” *Phys Rev Lett* **84**, 2064–2067 (2000).
- ²⁴ S. Torquato and F. H. Stillinger, “Local density fluctuations, hyperuniformity, and order metrics,” *Phys Rev E* **68**, 41113 (2003).
- ²⁵ A. Donev, F. H. Stillinger, and S. Torquato, “Unexpected Density Fluctuations in Jammed Disordered Sphere Packings,” *Phys Rev Lett* **95**, 90604 (2005).
- ²⁶ R. P. Kennan, J. Zhong, and J. C. Gore, “Intravascular Susceptibility Contrast Mechanisms in Tissues,” *Magn Reson Med* **31**, 9–21 (1994).
- ²⁷ P. Gillis, S. Petö, F. Moiny, J. Mispelster, and C. A. Cuenod, “Proton Transverse Nuclear Magnetic Relaxation in Oxidized Blood:

- a Numerical Approach,” *Magn Reson Med* **33**, 93–100 (1995).
- ²⁸ G. Deville, M. Bernier, and J. M. Delrieux, “NMR multiple echoes observed in solid ^3He ,” *Phys Rev B* **19**, 5666–5688 (1979).
- ²⁹ A. Gabrielli, M. Joyce, and F. Sylos Labini, “Glass-like universe: Real-space correlation properties of standard cosmological models,” *Phys Rev D* **65**, 83523 (2002).
- ³⁰ H. C. Torrey, “Bloch Equations with Diffusion Terms,” *Phys Rev* **104**, 563–565 (1956).
- ³¹ D. S. Novikov and V. G. Kiselev, “Effective medium theory of a diffusion-weighted signal,” *NMR Biomed* **23**, 682–697 (2010).
- ³² D. S. Novikov, M. Reisert, and V. G. Kiselev, “Effects of mesoscopic susceptibility and transverse relaxation on diffusion NMR,” *J Magn Reson* **293**, 134–144 (2018).
- ³³ R. Xie, G. G. Long, S. J. Weigand, S. C. Moss, T. Carvalho, S. Roroda, M. Hejna, S. Torquato, and P. J. Steinhardt, “Hyperuniformity in amorphous silicon based on the measurement of the infinite-wavelength limit of the structure factor,” *Proc Natl Acad Sci USA* **110**, 13250–13254 (2013).
- ³⁴ Y. Jiao, T. Lau, H. Hatzikirou, M. Meyer-Hermann, J. C. Corbo, and S. Torquato, “Avian photoreceptor patterns represent a disordered hyperuniform solution to a multiscale packing problem,” *Phys Rev E* **89**, 022721 (2014).
- ³⁵ R. Dreyfus, Y. Xu, T. Still, L. A. Hough, A. G. Yodh, and S. Torquato, “Diagnosing hyperuniformity in two-dimensional, disordered, jammed packings of soft spheres,” *Phys Rev E* **91**, 12302 (2015).
- ³⁶ M. Skoge, A. Donev, F. H. Stillinger, and S. Torquato, “Packing hyperspheres in high-dimensional Euclidean spaces,” *Phys Rev E* **74**, 41127 (2006).
- ³⁷ A. Savitzky and M. J. E. Golay, “Smoothing and Differentiation of Data by Simplified Least Squares Procedures,” *Anal Chem* **36**, 1627–1639 (1964).
- ³⁸ A. Ruh, H. Scherer, and V. G. Kiselev, “The Larmor Frequency Shift in Magnetically Heterogeneous Media Depends on Their Mesoscopic Structure,” *Magn Reson Med* **79**, 1101–1110 (2018).

Acknowledgements

AR, PE and V GK were supported by the German Research Foundation (DFG), grant KI 1089/6-1. DSN was supported in part by the Center of Advanced Imaging Innovation and Research (CAI2R, www.cai2r.net), a NIH/NIBIB Biomedical Technology Research Center: P41 EB017183, and by NIH/NINDS grants R01 NS088040 and R01 NS039135.

METHODS

Synthetic media. In Fig. 1, we consider five representative media: four types of differently arranged identical spheres with radius ρ , and one with randomly placed long (prolate) ellipsoids (here ρ is the radius of the short axes, the long semi-axis is 40ρ), which were generated as follows. A simple cubic lattice of spheres with a volume fraction of $\zeta = 34\%$ represents perfect order. To create the shuffled lattice, the spheres of the regular lattice were randomly displaced from their original positions by nine discrete values within the distance $\pm 0.2335\rho$ in each direction rejecting steps that caused overlap with a neighbor. The MRJ packing was generated using an event-driven molecular dynamics simulation³⁶ using the code downloaded from the authors’ website. The resulted medium had the volume fraction of spheres $\zeta = 65\%$. For the short-range disorder, the spheres

were randomly added rejecting steps leading to the overlap with already existing spheres ($\zeta = 34\%$). The same algorithm was used for the random arrangement of long ellipsoids whereas the non-overlap condition was released resulting the ellipsoids with the summed volume of 15% of the simulation volume forming a structure with the overall volume fraction $\zeta = 14\%$. To alleviate finite-size effects in the diverging power spectrum of the long ellipsoids at small k (Fig. 1), we further averaged the MC runs over ten different disorder realizations. All media were sampled on a 1024^3 cubic grid for numerical computation of $\Omega(\mathbf{r})$ and successive MC simulations.

The Larmor frequency shift, $\Omega(\mathbf{r})$, was calculated as the convolution with the elementary dipole field. To characterize the scale (the dephasing strength) of field variations, we use the dephasing introduced by a single object: $\delta\Omega = \frac{4}{3}\pi\chi\gamma B_0$ for spheres and $\delta\Omega = 2\pi\chi\gamma B_0$ for the long ellipsoids, where χ is the susceptibility difference with the background, and γB_0 the Larmor frequency in the external field. The disorder correlation length l_c was defined starting with $k_c = \pi/\rho$, which is close to the pronounced peak of $\bar{\Gamma}_2(k)$ for the considered sphere packings, correspondingly $l_c = 1/k_c$ and the correlation time $t_c = 1/(Dk_c^2)$. The dimensionless parameter $\alpha = \delta\Omega t_c$ instantiates the typical spin phase, $\langle\varphi_1^2\rangle$, acquired when moving over the disorder correlation length; the diffusion-narrowing takes place when $\alpha \ll 1$.

Numerical calculations to obtain $\Sigma(\omega)$ and $dR_2(t)/dt$ to the leading order were performed by integrating the Larmor frequency power spectra $\Gamma_2(\mathbf{k}) = \Omega_{-\mathbf{k}}\Omega_{\mathbf{k}}/V$, cf. Eq. (4), for the five synthetic media according to Eqs. (9) and (10), respectively, while neglecting R_2^∞ on the right-hand side.

Monte Carlo simulations of the mesoscopic relaxation for freely diffusing spins were performed with $N_s = 10^8$ spins randomly hopping on the sample grid of the above described media imitating the dephasing strength $\alpha = 0.2$ (spheres) and $\alpha = 0.05$ (long ellipsoids). The increment of the random walker’s spin phase was calculated using the mean of $\Omega(\mathbf{r})$ before and after each hop. The mesoscopic NMR signal at each time moment t was calculated as the mean of all accumulated phase factors $s(t) = \langle e^{-i\varphi(t)} \rangle$. The second derivative of $\ln s(t)$ was calculated using third-order polynomial fitting, based on Savitzky-Golay filtering,³⁷ with a linearly increasing filter width of $0.6t$.

Microbead samples. Polystyrene microbeads (Dynoseed TS10; Microbeads AS, Skedsmokorset, Norway) were suspended in an aqueous solution of sodium chloride doped with Holmium(III) chloride hexahydrate ($\text{HoCl}_3 \cdot 6\text{H}_2\text{O}$) in various concentrations to adjust the solution density and magnetic susceptibility, respectively.³⁸ Suspensions with 30% volume fraction of microbeads were prepared using a particle-density matched sodium chloride solution ($c_{\text{NaCl}} = 1.28 \text{ mol/L}$ for $T = 309 \text{ K}$) to avoid sedimentation. MRJ samples were prepared by particle sedimentation in $c_{\text{NaCl}} = 0.33 \text{ mol/L}$ solution and careful removal of particle-free fluid from the top. All samples were prepared in standard 5-mm NMR tubes.

NMR measurements were performed on a DPX 200 MHz spectrometer (Bruker, Ettlingen, Germany) using a standard zg30 sequence (flip angle = 30° , acquisition time = 4 s, 16 averages, relaxation delay = 3 s, no spinning) at $T = 309 \text{ K}$. The shim fields were adjusted on a pure D_2O sample and then kept for all samples within a measurement series. To obtain dR_2/dt , the measured FID signals were processed with the same fitting algorithm³⁷ as applied for MC simulations using a filter width of $0.7t$.

SUPPLEMENTAL INFORMATION

Monte Carlo simulations for hindered diffusion were performed within the same media and with the same parameters as in Fig. 1. Impermeable spheres and ellipsoids were simulated by discarding Monte Carlo steps that lead inside the objects in which case the random walkers did not move dur-

ing the given time step. The results shown in Fig. S1 support the universality of the dynamical exponent, while the coefficients in front of $t^{-\nu}$ and $|\omega|^{\nu-1}$ are non-universal. Note that the renormalization of the diffusion constant with its long-time asymptote (Fig. S2) is not sufficient to reproduce the non-universal coefficients (data not shown), which are strongly modified for the media with higher volume fraction ζ .

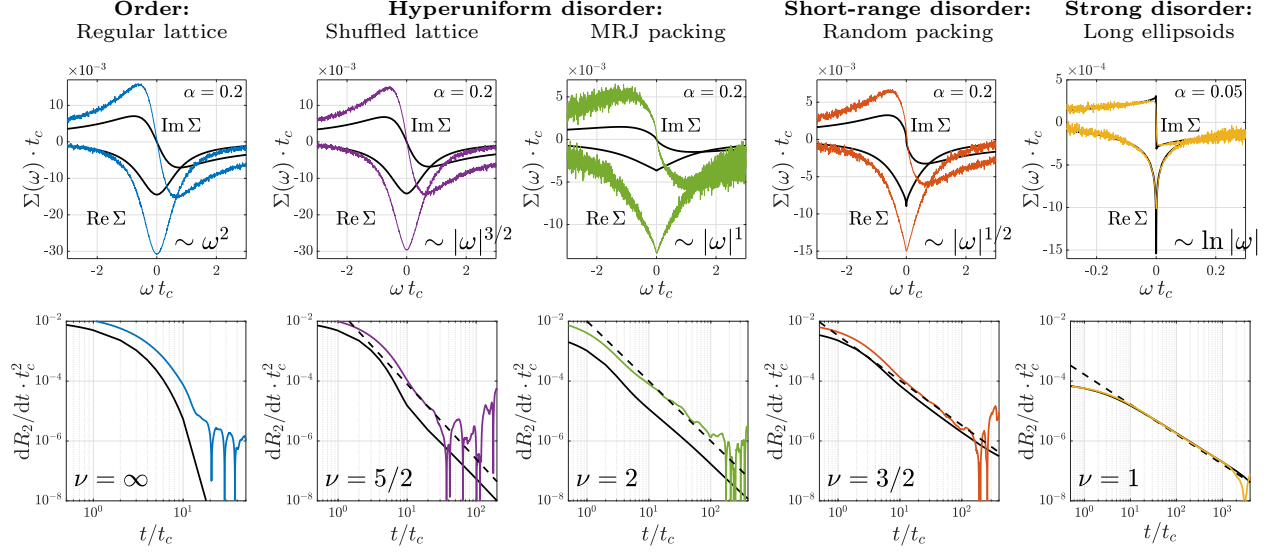


FIG. S1. Results for hindered diffusion in the five three-dimensional synthetic media from Fig. 1 representing different disorder classes. The second row shows the derivative of the time-dependent relaxation rate, dR_2/dt . MC results for hindered diffusion (colored curves) in general differ from the leading-order calculation (black curves, the same as in Fig. 1), which assumes permeable objects, but follow the same characteristic exponents (dashed lines). The same observation holds for the equivalent depiction in frequency domain (first row). While the self-energy curves also differ quantitatively from the leading-order calculation, the qualitative behavior embodied by the power-law exponent at $\omega = 0$ is similar. For strong disorder the difference between hindered and free diffusion is actually negligible, which follows from the low volume fraction of $\zeta = 14\%$ for the long ellipsoids.

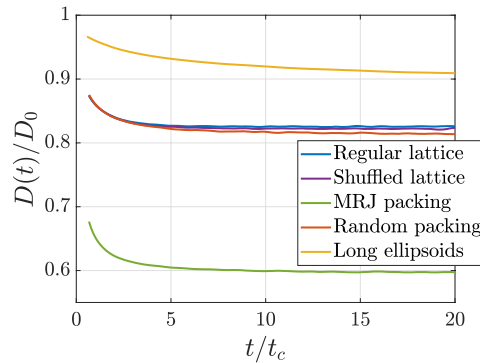


FIG. S2. Instantaneous diffusion coefficient³¹ $D(t) = \frac{1}{6} \partial_t \langle x^2(t) \rangle$ for the hindered diffusion within the investigated media, normalized to the free diffusion coefficient D_0 . The temporal derivative of the mean square displacement $\langle x^2(t) \rangle$ of the MC random walkers was computed using the Savitzky-Golay filter³⁷ based on the second-order polynomial, with a width of about t_c .